minerals

MDPI

Article

Metasomatic Reactions between Archean Dunite and Trondhjemite at the Seqi Olivine Mine in Greenland

Laura Whyatt [1], Stefan Peters [2], Andreas Pack [2], Christopher L. Kirkland [3], Tonci Balic-Zunic [1] and Kristoffer Szilas [1,*]

1 Department of Geosciences, University of Copenhagen, Øster Voldgade 10, 1350 Copenhagen K, Denmark; laurawhyatts@hotmail.com (L.W.); toncib@ign.ku.dk (T.B.-Z.)
2 Geosciences Centre, University of Göttingen, Goldschmidtstraße 1, 37077 Göttingen, Germany; speters2@gwdg.de (S.P.); Andreas.Pack@geo.uni-goettingen.de (A.P.)
3 Centre for Exploration Targeting—Curtin Node, The Institute for Geoscience Research, School of Earth and Planetary Sciences, Curtin University, Perth 6102, WA, Australia; C.Kirkland@curtin.edu.au
* Correspondence: krsz@ign.ku.dk

Received: 29 November 2019; Accepted: 19 January 2020; Published: 20 January 2020

Abstract: A metasomatic zone formed between the contact of a 2940 ± 5 Ma intrusive trondhjemite sheet in the Archean dunite of the Seqi Ultramafic Complex, SW Greenland, consists of three distinct mineral zones dominated by (1) talc, (2) anthophyllite, and (3) phlogopite. These zones supposedly resulted from a process of dissolution of olivine by silica rich fluid residual from the trondhjemite magma, with crystallization of secondary minerals along a compositional gradient in the fluid phase. A zircon crystal inclusion in a large (4 cm) olivine porphyroblast was dated in situ via LA-ICP-MS U–Pb isotope analysis, yielding a weighted mean $^{207}Pb/^{206}Pb$ age of 2963 ± 1 Ma, which coincides with granulite facies metamorphism and potential dehydration. Considering phase relations appropriate for the dunite composition, we deduced the talc forming conditions to be at temperatures of 600–650 °C and at a pressure below 1 GPa. This is supported by oxygen isotope data for talc, anthophyllite and phlogopite in the metasomatic zone, which suggests formation in the temperature range of 600–700 °C from fluids that had a $\delta^{18}O$ of ~8‰ and a $\Delta'^{17}O_{0.528}$ of about −40 ppm, i.e., from fluids that could have been derived from the late stage trondhjemite sheet.

Keywords: Archaean; Greenland; ultramafic rocks; metasomatism; talc; anthophyllite; phlogopite

1. Introduction

Metasomatism is the process of compositional change in a rock due to the removal and/or addition of chemical components during the interaction of a precursor rock with either melt or hydrous fluid. The main driver of metasomatic reactions is a chemical gradient between the rock and the fluid/melt phase, which leads to the exchange of components and therefore potentially phase transitions.

The Archean crust in the Nuuk region of SW Greenland ranges in age from 3.8 Ga tonalite to 2.5 Ga granite [1,2]. Interspersed with such evolved continental crust, are scattered enclaves of both mafic and ultramafic rocks, which range in size from decimeter to kilometer scale (Figure 1). These remnants of older crustal components in the Archean continental crust are dominated by mafic metavolcanic rocks [3], with lesser amounts of plutonic rocks, including anorthosite, gabbro, norite, and peridotite [4]. In addition, several crustal peridotite bodies, which represent large fragments and enclaves derived from layered complex of unknown age within the tonalitic orthogneiss, have been identified in SW Greenland in recent years (e.g., [5,6]).

The relationship between ultramafic rocks and the hosting continental crust is of specific interest due to their contrasting geochemical compositions and hence high chemical potential gradient at their contact. Contact zones between peridotite and felsic lithologies have previously been shown to result in unusual metasomatic minerals, including corundum, formed during high-grade metamorphic conditions [7,8].

In the present study, we investigated metasomatic reactions observed at the interface between Archean dunite and granitoid felsic sheets at the Seqi Olivine Mine, which led to the formation of phlogopite, anthophyllite, and talc with decreasing distance from the felsic intrusives. We combined mineralogical and geochemical data to examine the compositional changes and to characterize the element mobility during this metasomatic process at amphibolite facies conditions.

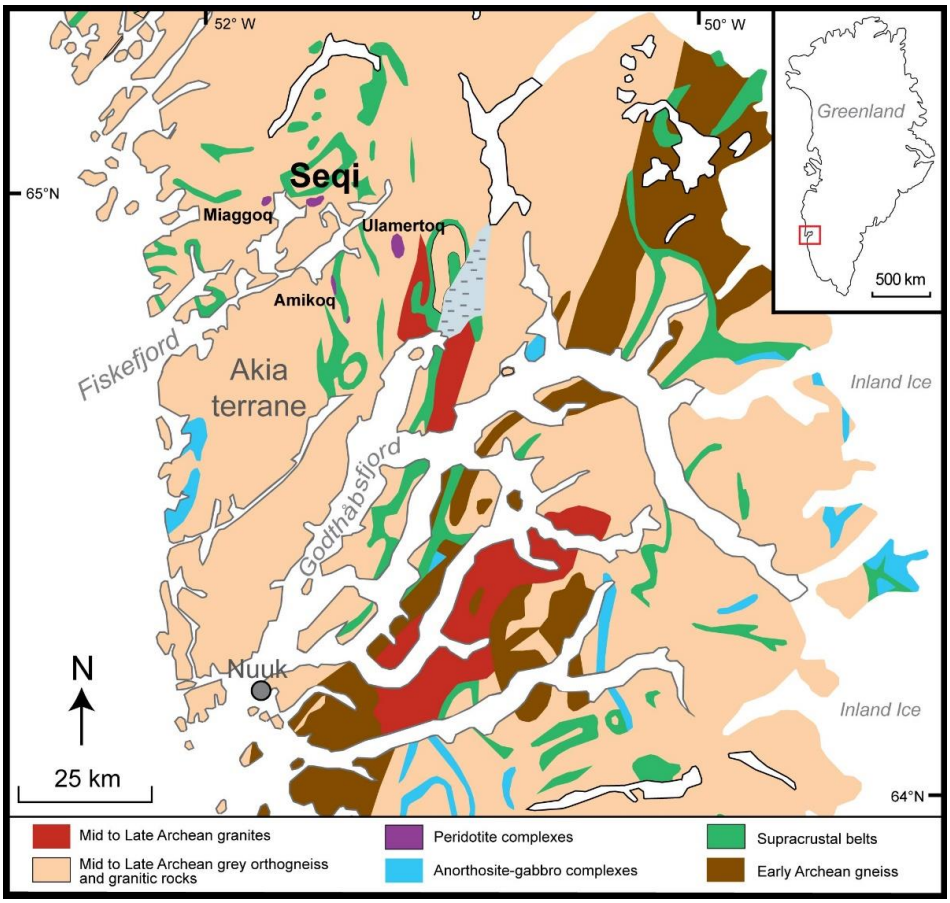

Figure 1. Geological map of the Nuuk region of SW Greenland consists of four main crustal terranes: Itsaq Gneiss Complex (3.8–3.6 Ga); Akia Terrane (ca. 3.2–3.0 Ga); Kapisilik Terrane (ca. 3.1–3.0 Ma); Tasiusarsuaq Terrane (2.92–2.84 Ga). The Seqi Olivine Mine is located at the end of Fiskefjord together with several similar Archean ultramafic bodies. Map modified after [9].

2. Geological Setting

The Nuuk region of SW Greenland hosts the largest expanse of Eoarchean continental crust anywhere on Earth, known as the Itsaq Gneiss Complex [1]. This orthogneiss complex forms the nucleus of the North Atlantic Craton, along which several Mesoarchean crustal terranes were amalgamated until their common stabilization at the end of the Archean Eon [10] (Figure 1).

One of these younger crustal blocks is the Mesoarchean Akia Terrane, which hosts the rocks of the present study. It formed during two distinct stages of crustal growth with an early 3.2 Ga dioritic core, and a ca. 3.0 Ga tonalitic phase [11–13]. The Akia Terrane was amalgamated to the Itsaq Gneiss

Complex at around 2.8–2.7 Ga [10], which was then followed by suturing of the contact by the intrusion of the Qôrqut Granite Complex at around 2.5 Ga [2].

Intercalated within the granitoid crust of the Akia Terrane are remnants of supracrustal/greenstone belts and layered ultramafic complexes [9,14,15]. One of the most prominent of the ultramafic bodies is the Seqi Ultramafic Complex [5], which is dominated by dunite, mined recently (between 2005 and 2010) for industrial grade olivine by the Swedish company Minelco. The Seqi Ultramafic Complex covers an area of approximately 0.5 km^2. The olivine mine open pit covers about a quarter of the exposed dunite body.

The various types of dunite in the Seqi complex are exceptionally fresh and exhibit well-equilibrated granoblastic metamorphic textures. The dunites only display vague retrogression as seen by the formation of chlorite along grain boundaries, with breakdown of chromite grains. In addition to such relatively late features are also evidence of higher grade metamorphism in the form of a large poikilitic orthopyroxene that overgrows aggregates of olivine (Figure 2a), amphibole veins (Figure 2b), and euhedral olivine porphyroblasts, which commonly preserve cores of actinolite (Figure 2c,d). These features attest to an early stage of hydration of the Seqi dunites, which was followed by widespread dehydration and re-equilibration of the ultramafic rocks.

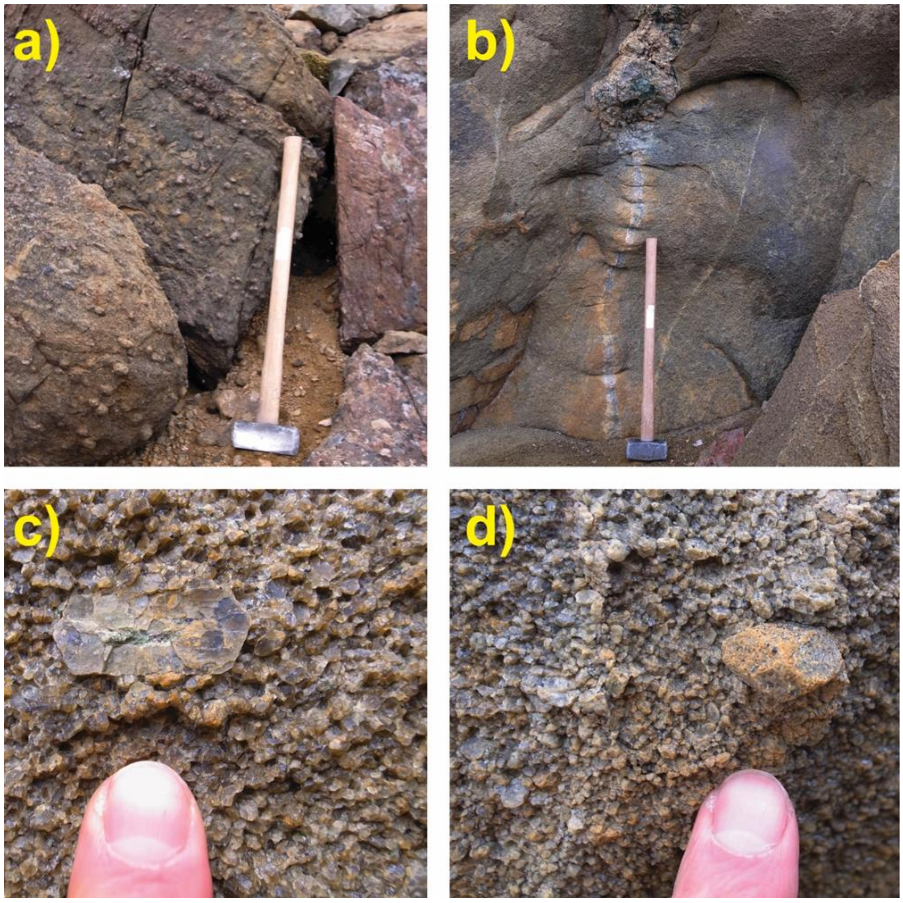

Figure 2. Field photos from the Seqi Ultramafic Complex. (**a**) Poikilitic dunite showing isolated poikiloblasts of coarse orthopyroxene with diameters up to 5 cm. (**b**) Example of actinolite-rich metasomatic vein in dunite. (**c**) Porphyroblastic dunite with a large (3 cm) euhedral olivine crystal, which is broken in half showing a core of actinolite. (**d**) Porphyroblastic dunite showing unbroken euhedral olivine crystal. Please see Szilas et al. [5] for further details on textures and rock types.

The minimum age of the Seqi complex is constrained by an intrusive tonalitic sheet at 2978 ± 8 Ma [5], coincident with the transition from continental crust formation to regional granulite

facies metamorphism in the Akia Terrane [16]. This event might indeed be responsible for the dehydration of the Seqi dunites. However, as we demonstrated in this study, there was also local infiltration of fluids and/melts during the intrusion of a felsic granitoid.

The present study focused on metasomatic reactions that are observed at the contact between late intrusive granitoid sheets and dunite within the Seqi Ultramafic Complex, such as the examples given in Figure 3. These contacts are associated with significant hydration of the protolith, with concomitant changes of the granitoid itself.

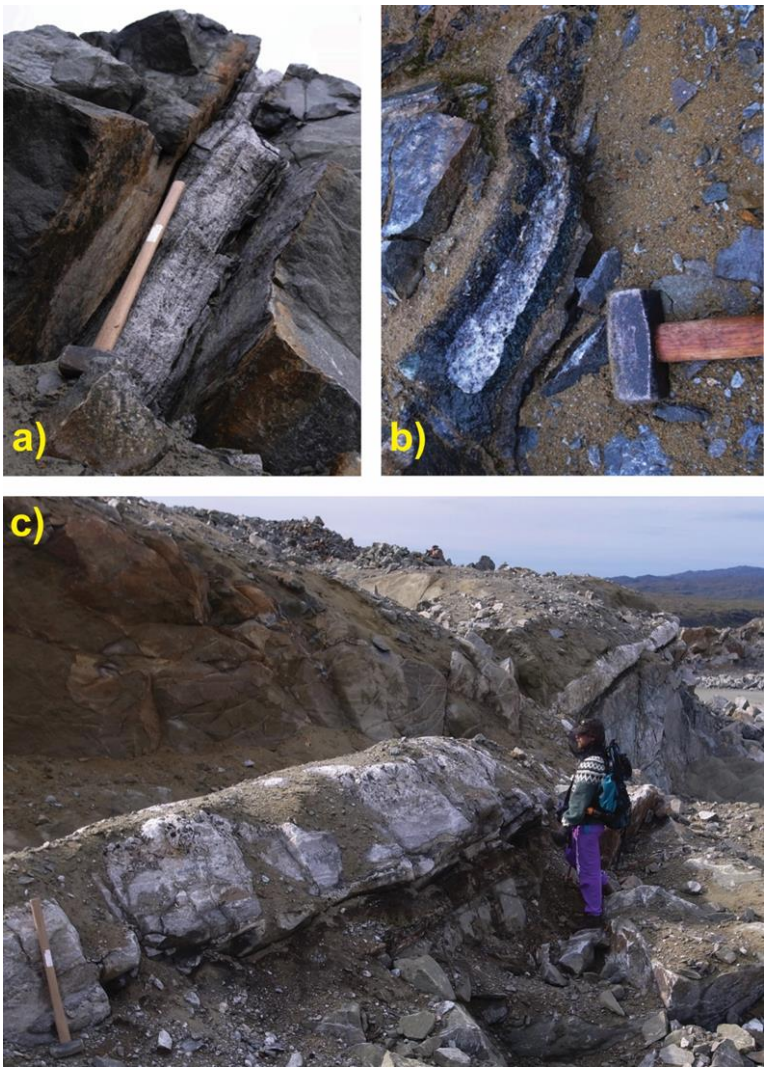

Figure 3. Field photos from the Seqi Olivine Mine showing examples of felsic intrusive sheets in dunite. (**a**) 40 cm thick intrusive tonalitic sheet (sample 186451), which was dated at 2963 ± 6 Ma [5]. Note the dark contact zone, which is dominated by talc and mica. (**b**) 20 cm felsic intrusive vein in dunite with obvious metasomatic reaction halo, which almost completely consumes the granitoid rock. (**c**) Large (1.5 m) NE–SW trending trondhjemitic pegmatite sheet (sample 186453) in the central part of the Seqi Olivine Mine pit.

3. Materials and Methods

3.1. Samples and Petrography

The samples used in the present study are from the Seqi Olivine Mine [5], and include the contact zone between refractory cumulate dunite (represented by sample 186452) and intrusive granitoid pegmatite (represented by sample 186453, Figure 3c). The latter granitoid pegmatite was previously

dated at 2940 ± 5 Ma by LA-ICP-MS (Laser Ablation Inductively Coupled Plasma Mass Spectrometry) U–Pb in zircon [5]. Our analyses showed that the pegmatite is dominated by albitic plagioclase, and is therefore classified as trondhjemite.

The studied metasomatic reaction consists of three mineral associations going from a mica-rich proximal zone at the pegmatite side, to a fibrous white amphibole zone, and finally a talc-dominated zone on the dunite side of the reaction front (Figure 4). Microscopy showed elongated, fibrous, colorless mineral with high relief, occurring in all three metasomatic zones (Figure 5c). This mineral was identified by X-Ray Diffraction (XRD) and Electron Microprobe Analysis (EMPA) as anthophyllite. A colorless mineral with a low relief, was also present in most of the samples and was identified as talc (Figure 5a). A brown to yellowish flaky mineral with a low relief, was also present throughout the metasomatic zone (Figure 5d), and was identified as phlogopite. Opaque minerals appeared as a minor phase (Figure 5b,c) and were identified as spinel (chromite and magnetite) by EMPA analysis.

The host dunite was previously described in detail by Szilas et al. [5]. Although several textural types occur in the Seqi olivine mine, the main one can be described as being texturally homogeneous with unserpentinized olivine having well-equilibrated granoblastic annealing texture with 120° angles between the grains (Figure 5a), consistent with the high-grade granulite facies metamorphic conditions that were documented for this region [12,16].

The talc zone (Figures 4 and 5b) is predominately talc (plastically deformed finer grains) in combination with some lepidoblastic anthophyllite. Opaque minerals occur as small partially digested grains (Figure 6a). Flaky/nematoblastic mica is present (weak greenish-yellow pleochroism), but to a lesser degree than anthophyllite. Olivine relicts are rarely observed.

The amphibole zone (Figure 5c) is dominated by oriented aggregates of fibrous anthophyllite crystals growing perpendicular to the contact plane (Figures 4 and 6b) with minor amounts of irregular to rounded opaque inclusions. This zone has a gradational transition into the mica zone, and anthophyllite mingles with broader phlogopite grains (green-colorless pleochroism) with successive disorientation of the grains.

The transitional mixture of anthophyllite and phlogopite with minor amounts of talc gives way to mica (phlogopite) with a weak greenish-yellow pleochroism. This mica zone (Figures 5d and 6c) eventually becomes entirely dominated by phlogopite.

Additionally, a zircon grain was identified within a euhedral olivine porphyroblast in dunite sample 186460. The zircon was dated by in situ U–Pb isotope analyses using the LA-MC-ICP-MS method (laser ablation multi-collector inductively coupled plasma mass spectrometry).

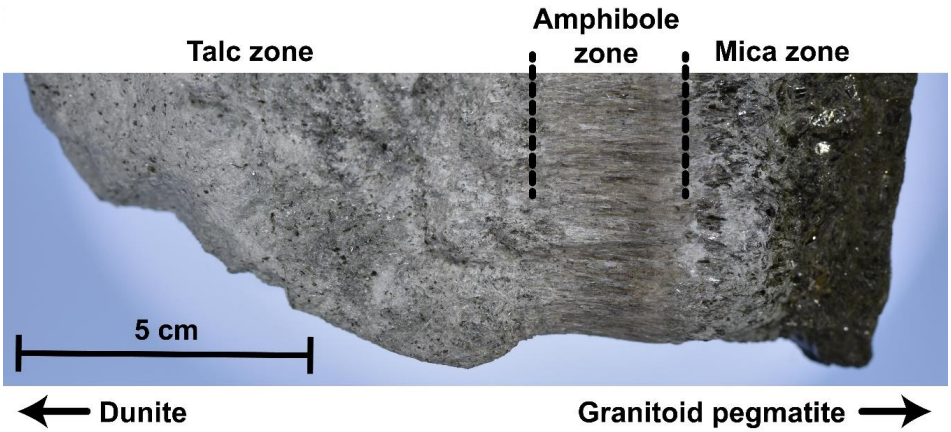

Figure 4. From right to left: trondhjemitic pegmatite (not visible), proximal mica zone, fibrous white amphibole zone (anthophyllite), talc-dominated zone, dunite (not visible), which is the dominant rock type of the Seqi Ultramafic Complex.

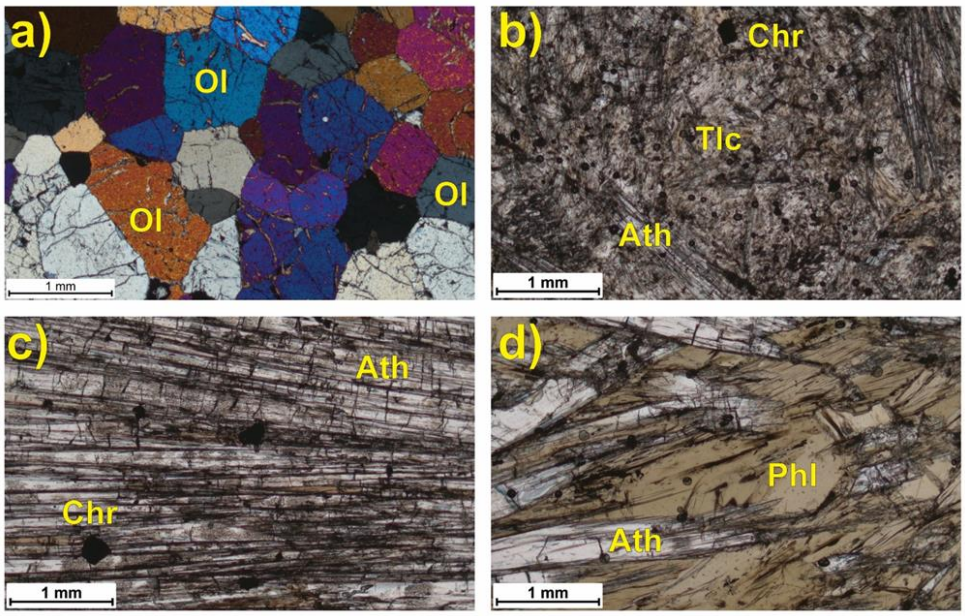

Figure 5. Microphotographs of the some of the samples of the present study. (**a**) Granoblastic dunite with distinct metamorphic texture in cross-polarized light. (**b**) Talc-dominated metasomatic rock with small specs of chromite and fibrous anthophyllite seen in plane polarized light. (**c**) Coarse fibrous and strongly parallel anthophyllite with rare euhedral chromite grains seen in plane polarized light. (**d**) Mica-dominated metasomatic rock at the contact to the granitoid intrusive sheet. Amphibolite needles (anthophyllite) are present towards the dunite side of the reaction, whereas biotite dominates the trondhjemite side of the metasomatic zone. Thin section image seen in plane polarized light. Abbreviations: Ant (anthophyllite), Chr (chromite), Phl (phlogopite), Ol (olivine), Tlc (talc).

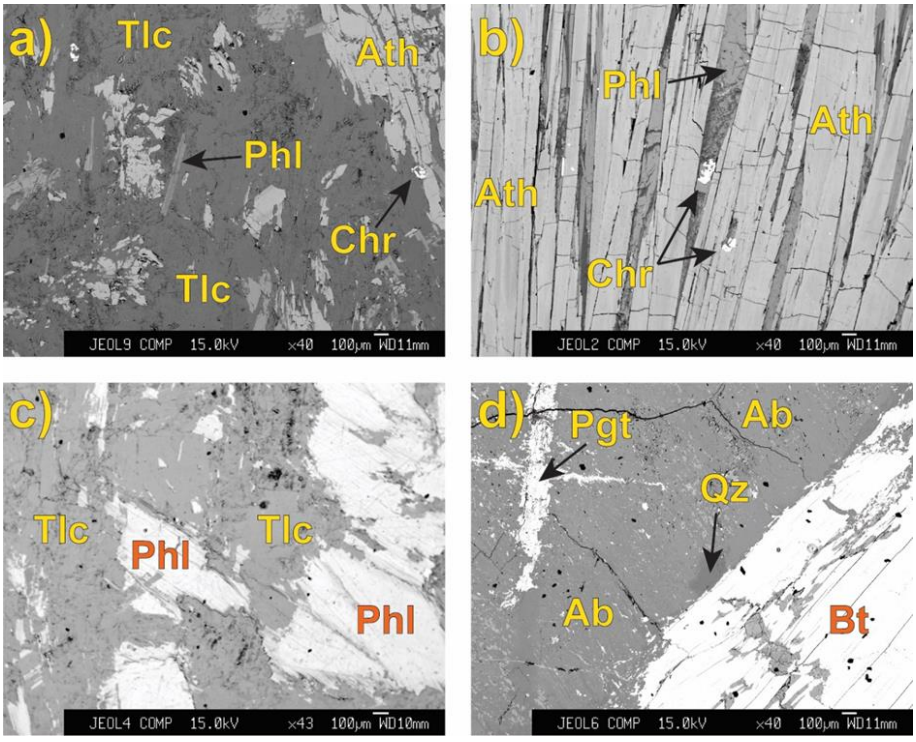

Figure 6. Back-scattered electron (BSE) images of the Seqi samples. (**a**) Talc zone; (**b**) Amphibole zone; (**c**) Mica zone; (**d**) Trondhjemitic pegmatite. Abbreviations: Ab (albite), Ant (anthophyllite), Bt (biotite), Chr (chromite), Pgt (pigeonite), Phl (phlogopite), Tlc (talc).

3.2. Methods

3.2.1. Bulk-Rock Geochemical Data

Bulk-rock major and trace element data were acquired from the geochemical laboratory at Washington State University (WSU, Pullman, WA, USA). The procedure involves flux fusion digestion of rock powders followed by routine XRF (X-Ray Fluorescence) and ICP-MS analysis. Potential contamination from the Li-tetraborate flux was corrected for by a blank subtraction. The full analytical procedures are described on WSU's website and the reader is referred to this for additional details [17].

3.2.2. Electron Microprobe Analysis

Electron Microprobe Analysis (EMPA) was conducted using a JEOL JXA8200 at the University of Copenhagen (Copenhagen, Denmark). A beam current of 15 nA, acceleration voltage of 15 kV, and spot size of 5µm was used. The counting time was set for 20 s for each element, except for sodium and potassium, for which 10 s was used. The elements chosen for the analysis were silicon (Si), manganese (Mn), potassium (K), chromium (Cr), sodium (Na), aluminum (Al), iron (Fe), calcium (Ca), nickel (Ni), magnesium (Mg), and titanium (Ti) using the standardization described by [18].

3.2.3. Powder X-ray Diffraction

The powder x-ray diffraction (PXRD) instrument used in this investigation was a Bruker-AXS D8 Advance diffractometer with a primary Ge111 monochromator and a LinxEye silicon-strip detector with an active surface covering 3.3° located at the University of Copenhagen (Copenhagen, Denmark). The used radiation was from a sealed Cu tube (1.54059 Å). The measurements were made between 5 and 90° 2θ, in steps of 0.02° and a measuring time of 4 s. The reflection Bragg-Brentano technique was used with sample rotation and a fixed divergence at 0.25°. Sample preparation included crushing samples to a grain size of less than 45 µm, and mounting the powder in a metal sample holder with a cavity of 2 mm depth.

Mineral identification was done using an own database with mineral diffraction data and refined with a help of Topas6 Software (version 1, 2017, Bruker AXS, Billerica, MA, United States) using the Rietveld method, with a simultaneous quantitative analysis of mineral proportions.

3.2.4. Triple Oxygen Isotope Analysis

The triple O isotope compositions ($\delta^{17}O$, $\delta^{18}O$) of samples from the intrusive granitoid pegmatite, the talc zone, the antophyllite zone, and the mica zone were determined using the analytical setup at the University of Göttingen, Germany [19]. Two samples of the refractory dunite were analyzed for their triple O isotope compositions as well. For each sample, approximately 2.2 mg of material was reacted with excess BrF_5 by laser heating in a stainless-steel sample chamber. The O_2 that was produced by the reaction was cleaned from contaminant gasses by, respectively, distillation at −196 °C (e.g., BrF_5), reaction with NaCl (F_2) followed by distillation (Cl_2), and with a gas chromatograph (e.g., N_2, NF_3). The $\delta^{17}O$ and $\delta^{18}O$ values of the sample O_2 were then determined with a MAT 253 gas source mass spectrometer in dual inlet mode, relative to a reference gas of which the composition was determined relative to the VSMOW2 water standard [19].

The triple O isotope compositions of the samples are expressed below with the parameter $\Delta'^{17}O_{0.528}$, which denotes the deviation of the linearized $\delta^{17}O$ at the linearized $\delta^{18}O$ of the sample, relative to a reference line lambda (λ) with a slope of 0.528 (e.g., [20,21]. The samples were analyzed together with UWG-2 garnet [22] and San Carlos olivine as external reference materials. The average $\delta^{18}O$ and $\Delta'^{17}O_{0.528}$ values of UWG-2 garnet ($\delta^{18}O$ = 5.74‰; $\Delta'^{17}O_{0.528}$ = −56 ppm) and San Carlos olivine ($\delta^{18}O$ = 5.45‰; $\Delta'^{17}O_{0.528}$ = −49 ppm) that were analyzed together with the samples are in good agreement with the long-term average values for these reference materials from our labs. The material of San Carlos olivine that was analyzed in this study was sampled from a different olivine crystal than

the material that was analyzed by [19], and had a higher $\delta^{18}O$ than the material in the [20] by ~0.2‰ relative to UWG-2 garnet.

3.2.5. Zircon U–Pb Isotope Analysis

U–Pb isotopes were measured using a Nu Plasma II multi-collector ICPMS with high purity Ar as the plasma gas (flow rate 0.98 L min^{-1}) at Curtin University, Bentley, Australia. During time-resolved processing, contamination resulting from inclusions and compositional zoning was monitored, and only the relevant part of the signal was integrated. The primary reference material used for U–Pb dating in this study was zircon standard OG1 (3465.4 ± 0.6 Ma [23]), which has an ablation response similar to the Archean grain of interest. Secondary standard zircon 91500 (1062.4 ± 0.4 Ma [24], GJ-1 (601.7 ± 1.4 Ma [25]), and Plešovice (337.13 ± 0.37 Ma [26]) yielded $^{206}Pb/^{238}U$ ages within 1% of the accepted value when reduced using appropriate matrix matched standards. The time-resolved mass spectra were reduced using the U–Pb Geochronology data reduction schemes in IoliteTM [27], and in-house Microsoft Excel macros. No common lead corrections were deemed necessary due to generally low ^{204}Pb counts. All ages are reported with ±2σ uncertainties unless specifically stated otherwise.

4. Results

4.1. Bulk-Rock Geochemical Data

The three reaction zones (Figure 4) were measured for their bulk-rock major and trace element compositions for comparison with the intrusive trondhjemite sheet and the host dunite. The data for the latter were previously reported by Szilas et al. [5] and are thus not presented in Supplementary Table S1, but are included for reference in the geochemical diagrams.

The trondhjemite sample has the highest SiO_2 and Al_2O_3 contents of the samples, with values of 83.23 wt.% and 9.96 wt.%, respectively. This is consistent with the predominance of quartz and albite in this sample, which also explain the high Na_2O content of 4.64 wt.% (Figure 7). It should be noted that it is difficult to obtain an average sample of the sheet because of relatively large crystals of albite and quartz. The sample used for the whole rock chemical analysis evidently contained more quartz than the one used for the PXRD analysis. According to the latter one the amounts of SiO_2, Al_2O_3, and Na_2O are 61.58, 23.77, and 14.40 wt.%, respectively, due to a significantly higher content of albite (80.5 wt.%) and a lower content of quartz (19 wt.%), which is consistent with the pegmatitic nature of this sample. In terms of trace element abundances, the pegmatitic trondhjemite has low contents of compatible elements, as expected (Figure 8). The trace element pattern of the trondhjemite sample is quite typical of the continental crust, with the exception that this sample has a strong negative anomaly of P_2O_5, in addition to the typical negative anomalies of Nb and TiO_2 (Figure 9).

The three metasomatic zones (talc, anthophyllite, and phlogopite) have quite comparable bulk-rock major element compositions, with a few distinct features. In terms of their SiO_2 and MgO content, they plot intermediate between the dunite and granitoid endmembers (Figure 7). The amphibole zone is notably enriched in FeO^T (9.74 wt.%) and MnO (0.584 wt.%) in comparison to all other measured samples. In contrast, the mica zone is enriched in K_2O (4.62 wt.%) and TiO_2 (0.077 wt.%), as well as in all incompatible trace elements to the point where it exceeds the abundances in even the trondhjemite sample (Figure 9). However, this might be due to a non-representative choice of the sample of trondhjemite, as mentioned before. The talc zone is comparable to the host dunite in most aspects, except for having significantly higher SiO_2 (60.87 wt.%) and lower MgO (29.80 wt.%). Surprisingly, Ni, V, and Sc are lower in the talc zone, but Cr is high, in comparison with the Seqi dunite (Figure 8). The talc zone is also enriched in K_2O, Cs, Rb, Pb, as well as, U (Figure 9).

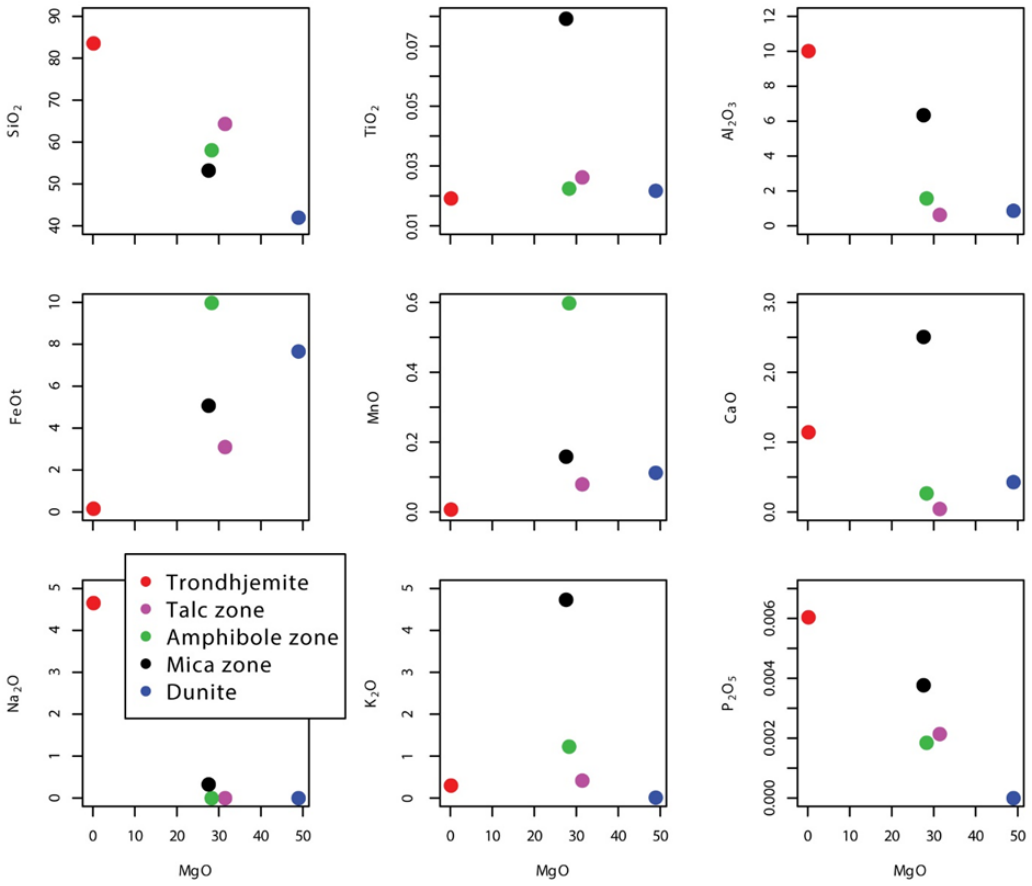

Figure 7. Major elements plotted against MgO contents for the samples of this study. The three metasomatic zones generally plot intermediate between the dunite and trondhjemite, which form compositional endmembers. The mica zone diverges from this trend by having significantly higher K_2O, CaO, and TiO_2 than the rest of the samples. Please note that the data for the dunite sample are from [5]. All oxides are given in wt.%.

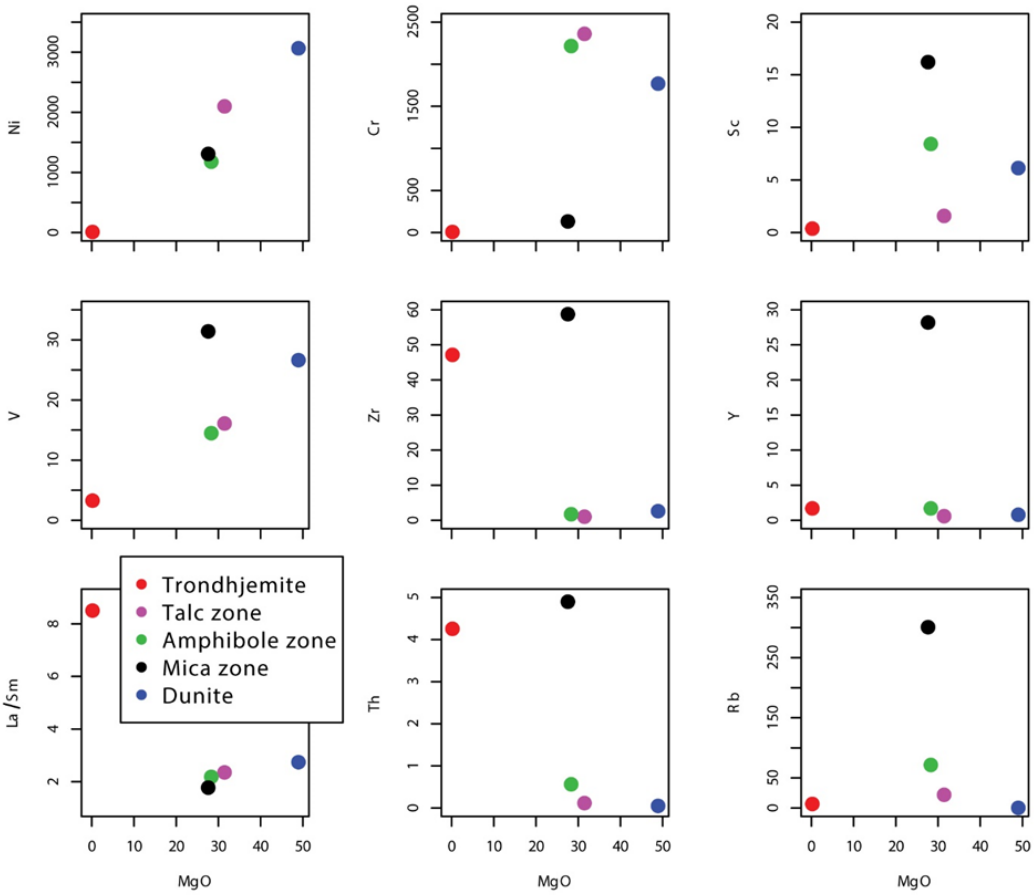

Figure 8. Trace elements plotted against MgO contents for the samples of this study. Like for the major elements shown in Figure 7, the three metasomatic zone roughly fall on a trend between the dunite and trondhjemite as the endmembers. The mica zone show deviation by having elevated Sc, V, Zr, Y, Th, and Rb. All traces elements are given in ppm.

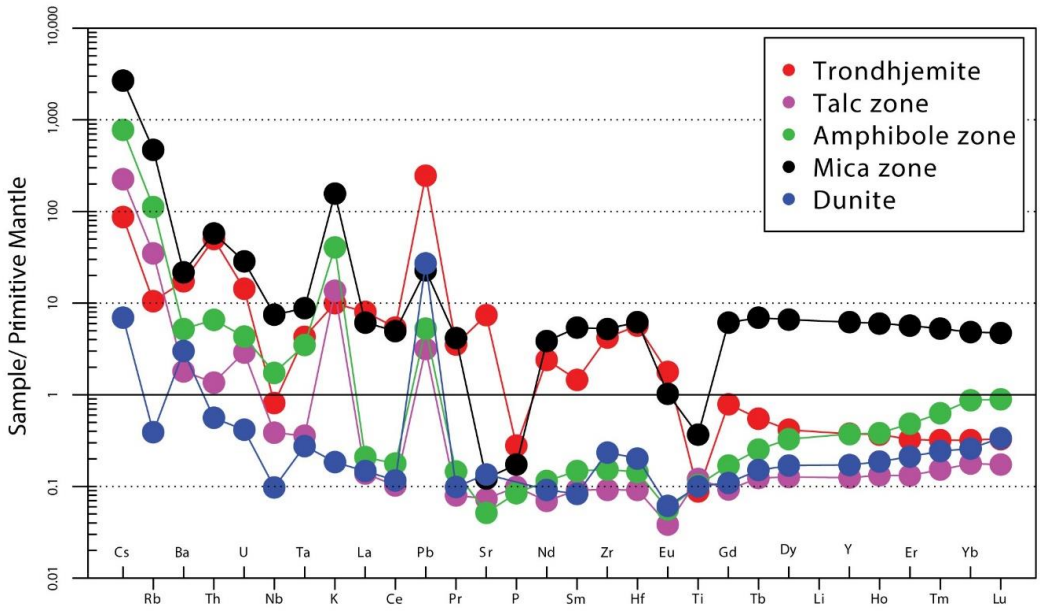

Figure 9. Incompatible trace element diagram normalized to primitive mantle [28]. The dunite, talc and amphibolite samples have the lowest abundances, whereas the mica sample has significantly elevated heavy rare earth element contents and otherwise resembles the granitoid sample.

4.2. Electron Microprobe Analysis

The three reaction zones, and the intrusive trondhjemite were studied by EMPA. The dunites of the Seqi Ultramafic Complex were previously described by Szilas et al. [5], so we refer the reader to that study for more details on the host dunite. Below we outline the results of the main minerals that were observed in the different reaction zones (Tables 1–4). The full EMPA data (wt.%) are presented in the Supplementary Table S2.

Table 1. The average mineral compositions from the talc zone (see Figure 6a).

Formula	Sites	Mineral
$Na_{0.01}(Ca_{0.04}Mg_{5.36}Mn_{0.1}Fe_{1.42}Ni_{0.03})Si_{8.01}O_{22}(OH)_2$	Σ A(0.01), M(6.95), T(8.01)	Anthophyllite
$(Cr_{1.61}Fe_{1.36}Al_{0.08}Mg_{0.05}Mn_{0.04}Ti_{0.01})O_4$	Σ M(3.15)	Chromite
$(K_{0.72}Na_{0.05}Ca_{0.02})(Mg_{2.67}Fe_{0.25}Al_{0.02}Cr_{0.02}Ni_{0.02}Ti_{0.01})(Si_{3.09}Al_{0.91})O_{10}(OH)_2$	Σ A(0.79), M(2.99), T(4)	Phlogopite
$(Mg_{2.81}Fe_{0.09}Al_{0.01}Ni_{0.03})Si_{4.03}O_{10}\ (OH)_2$	Σ M(2.94), T(4.03)	Talc

Table 2. The average mineral compositions from the amphibole zone (see Figure 6b).

Formula	Sites	Mineral
$Na_{0.01}(Ca_{0.05}Mg_{5.36}Fe_{1.38}Mn_{0.08}Ni_{0.03}Al_{0.01})Si_{8.05}O_{22}(OH)_2$	Σ A(0.01), M(6.85), T(8.05)	Anthophyllite
$(Cr_{1.51}Fe_{1.45}Al_{0.11}Mg_{0.06}Mn_{0.04}Ti_{0.01})O_4$	Σ M(3.18)	Chromite
$(K_{0.82}Na_{0.05}Ca_{0.01})(Mg_{2.65}Fe_{0.26}Ni_{0.02}Al_{0.02}Cr_{0.03}Ti_{0.01})(Al_{0.94}Si_{3.06})O_{10}(OH)_2$	Σ A(0.88), M(2.99), T(4)	Phlogopite
$(Mg_{2.81}Fe_{0.1}Ni_{0.03})Si_{4.01}O_{10}(OH)_2$	Σ M(2.94), T(4.01)	Talc

Table 3. The average mineral compositions from the mica zone (see Figure 6c).

Formula	Sites	Mineral
$(K_{0.84}Na_{0.05}Ca_{0.01})(Mg_{2.66}Fe_{0.26}Ni_{0.02}Al_{0.03}Ti_{0.01})(Al_{0.94}Si_{3.06})O_{10}(OH)_2$	Σ A(0.9), M(2.98), T(4)	Phlogopite
$(Na_{0.01}Mg_{2.85}Fe_{0.11}Ni_{0.02}Al_{0.01})Si_{3.99}O_{10}(OH)_2$	Σ M(3), T(4)	Talc

Table 4. The average mineral compositions from the trondhjemite (see Figure 6d).

Formula	Sites	Mineral
$(Na_{0.90}Ca_{0.12}K_{0.01})(Si_{2.88}Al_{1.10})O_8$	Σ A(1.03), T(3.98)	Albite
$(K_{0.93}\ Na_{0.01})(Mg_{1.45}Fe_{1.07}Al_{0.20}Ti_{0.12}Mn_{0.01})(Si_{2.88}Al_{1.12})O_{10}(OH)_2$	Σ A(0.94), M(2.85), T(4)	Biotite
$K_{0.01}(Na_{0.05}Ca_{1.89}Mg_{3.87}Fe_{1.04}Al_{0.1})Si_8O_{22}(OH)_2$	Σ A(0.01), M(6.95), T(8)	Tremolite
SiO_2		Quartz

4.3. Powder X-ray Diffraction

The results of PXRD are represented in Table 5 and diffractograms with results of the Rietveld refinement can be seen in the Supplementary Figures S1–S4. It is important to note that XRD gives a number of electrons for a structural site, without element speciation. It is thus possible to express simultaneous occupancies for only two chemical elements at a time unless crystal chemical parameters (e.g., bond lengths) are involved, which is practically feasible only for single crystal studies, not for PXRD on mineral mixtures. In the present cases, the main components in solid solutions at various structural sites were Mg and Fe, so the number of electrons for mixed sites was interpreted as due to Mg/Fe proportions and this is reflected in the calculated formulae.

It can be seen that mineral compositions and mineral proportions in the talc and amphibole zone correspond well with the EMPA (Tables 1 and 2) and the bulk chemical analysis. In the mica zone; however, the amphibole registered by PXRD is tremolite and not anthophyllite. This can be explained by the fact that this zone was analyzed close to the amphibole zone in EMPA (both zones were present in the polished section), whereas for PXRD a sample further away from the contact was taken in order to get a cleaner picture of this zone. Bulk-rock geochemical analysis, which shows significant Ca content, supports the PXRD results.

Table 5. Mineral compositions and proportions obtained by a Rietveld refinement of the PXRD data.

Talc Zone	Formula	wt.%
Talc	$Mg_{2.9}Fe_{0.1}Si_4O_{10}(OH)_2$	93.7
Anthophyllite	$Mg_{5.76}Fe_{1.24}Si_8O_{22}(OH)_2$ *	0.5
Phlogopite	$KMg_{2.76}Fe_{0.24}AlSi_3O_{10}(OH)_2$	5.8
Amphibole Zone	**Formula**	**wt.%**
Talc	$Mg_{2.8}Fe_{0.2}Si_4O_{10}(OH)_2$	1
Anthophyllite	$Mg_{5.76}Fe_{1.24}Si_8O_{22}(OH)_2$	92
Phlogopite	$KMg_{2.76}Fe_{0.24}AlSi_3O_{10}(OH)_2$	7
Chromite	Cr_2FeO_4 *	<0.1
Mica Zone	**Formula**	**wt.%**
Talc	$Mg_{2.9}Fe_{0.1}Si_4O_{10}(OH)_2$	4
Phlogopite	$KMg_{2.93}Fe_{0.07}Al_{1.19}Si_{2.81}O_{10}(OH)_2$	61.3
Tremolite	$Ca_{1.84}Fe_{0.08}Mg_5Si_8O_{22}(OH)_2$	34.5
Chlorite	$Mg_3Fe_3Al_{1.39}Si_{2.61}O_{10}(OH)_8$	0.2

* The composition was not refined due to a small quantity.

4.4. Triple Oxygen Isotope Analysis

The oxygen isotope compositions of the samples are given in Table 6. The $\delta^{18}O$ and $\Delta'^{17}O_{0.528}$ values of the trondhjemite sample are typical for evolved igneous rocks, and so are the triple O isotope compositions of the minerals from the metasomatic zones (e.g., [21,29]). The $\delta^{18}O$ and $\Delta'^{17}O_{0.528}$ of two dunite samples are similar to $\delta^{18}O$ and $\Delta'^{17}O_{0.528}$ of olivine in mantle peridotites (e.g., [19,20,30]).

Table 6. Triple oxygen isotope compositions. Measurement precisions (1 S.D.) are ±0.15‰ and ±10 ppm for $\delta^{18}O$ and $\Delta'^{17}O_{0.528}$, respectively, based on the repeated analysis of UWG-2 garnet and San Carlos olivine.

Sample	$\delta^{17}O$ [‰]	$\delta^{18}O$ [‰]	$\Delta'^{17}O_{0.528}$ [ppm]
186452 Dunite	2.71	5.19	−27
186478 Dunite	2.66	5.11	−43
208001 Talc zone	3.34	6.40	−37
208002 Amphibole zone	3.21	6.17	−40
208003 Mica zone	2.94	5.65	−33
186453 Trondhjemite	4.57	8.76	−43

4.5. Zircon U-Pb Isotope Analysis

One large zircon grain (length = 250 µm), included within olivine from Seqi dunite sample 186460, was targeted for U–Pb geochronology and a concordia plot is presented in Figure 10 below (see sample image in Supplementary Figure S5). This grain was spot ablated 26 times using a 22 µm spot across the exposed polished surface. Analyses indicated moderate to high U content of 220 to 609 ppm and relatively consistent Th/U ratios of around 0.2. All analyses were within 5% of Concordia and yield a weighted mean $^{207}Pb/^{206}Pb$ age of 2963 ± 1 Ma (n = 22; MSWD = 1.8; see Supplementary Figure S6). Because we did not observe any systematic age variation across the zircon grain, this age was interpreted as the age of magmatic crystallization of a metasomatic component incorporated into this rock. The U–Pb isotope data are reported in the Supplementary Table S3.

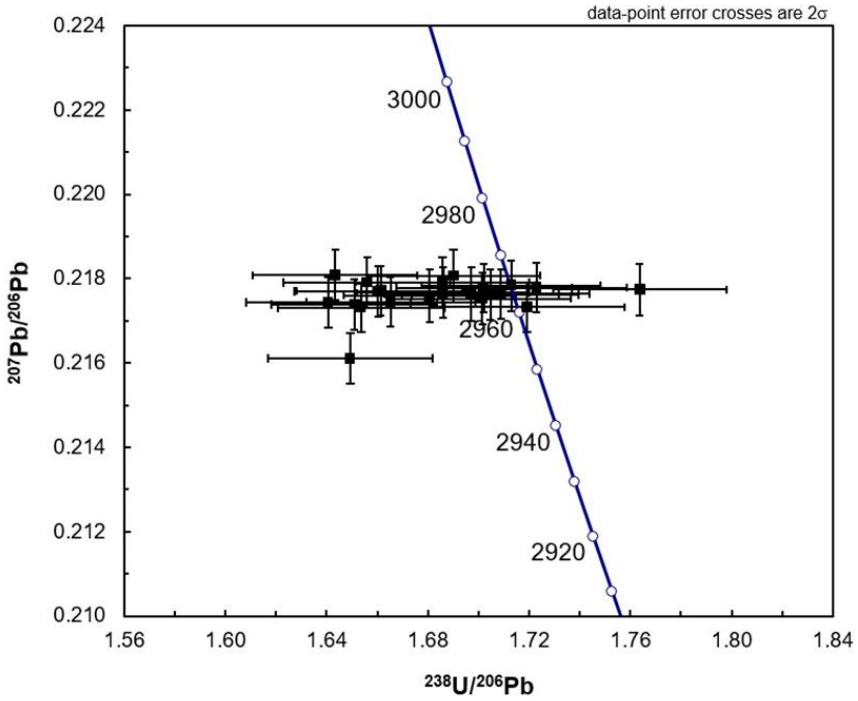

Figure 10. U–Pb isotope data from zircon measured in situ in porphyritic dunite sample 186460, yielding a weighted age of 2963 ± 1 Ma. This age represents a maximum age of the talc formation.

5. Discussion

5.1. Pressure-Temperature-Time Constrains of Talc Fomation

Studies of the Ulamertoq ultramafic body (Figure 1) indicated that the peridotites of the Fiskefjord region, which Seqi is part of, potentially experienced serpentinization followed by complete dehydration [31,32]. This is supported by the occurrence of humite-group minerals, and the commonly observed magnetite inclusions in olivine. Thus, the metamorphic history of the studied rocks is potentially quite complicated. The various textural types of Seqi dunite also contain magnetite inclusions, and previous serpentinization of these rocks can therefore not be excluded. However, it should be noted that the oxygen isotope compositions of the Seqi olivine is within the range of magmatic rocks, which places constraints on the degree of potential early serpentinization. The timing of talc formation at Seqi is not well defined, but must certainly postdate the 2990 Ma high temperature granulite facies event in the Akia Terrane, which caused extensive dehydration [11].

Kirkland et al. [33] used U–Pb isotope dating of apatite, which has a closure temperature of 375 to 600 °C [34,35], to provide constraints on the lower temperature evolution of the Akia Terrane. That study found evidence for thermal events ranging in age from ca. 2.8 to 1.8 Ga. We can rule out talc formation during the younger part of this period, because regional events from about 2.4 to 1.8 Ga were marked by mafic dyke swarms, which only had very localized alteration that was associated with low grade epidote and sericite [36].

The Nuuk region was characterized by terrane amalgamation from around 2.8 to 2.7 Ga [10,37], followed by crustal scale shear zone development at ca. 2.6 Ga [38,39], and finally deep crustal anataxis and injection of the Qôrqut Granite Complex at 2550 Ma [2]. The two latter events would both have been likely to cause significant fluid infiltration in the crust causing metasomatism; however, only the granite injection has documented meteoric water signatures in the form of low $\delta^{18}O$ in zircon.

The U–Pb isotope data for zircon included in olivine presented in this study demonstrated a thermal event at 2963 ± 1 Ma, which is consistent with previous zircon ages obtained for granitoid sheets within the Seqi Olivine Mine of 2978 ± 8 Ma (host tonalite), 2963 ± 6 Ma (intrusive tonalite sheet), and 2940 ± 5 Ma (granitoid pegmatite) [5]. We interpreted this zircon grain to have crystallized

during metasomatism and melt infiltration into the ultramafic body, because preliminary Re–Os age of ca. 3.3 Ga of the Seqi Ultramafic Complex [40] rules out a xenocrystic origin of the zircon grain. This is also obvious, because the tonalitic protolith of the regional TTG (tonalite–trondhjemite–granodiorite) gneiss formed between 3050–3000 Ma [13]. The lack of any systematic age correlation across the zircon grain also rules out resetting of the grain by Pb-loss. The fact that this zircon crystal was found within a porphyroblastic olivine grain indicates that the dunites of the Seqi Ultramafic Complex experienced metasomatism associated with the intrusion of granitoid sheets at temperatures above 700 °C, which represents the boundary between olivine and serpentine/talc stability for the Seqi bulk-rock compositions [5]. These conditions are in agreement with the regional P–T–t evolution indicating granulite facies metamorphism from around 2990–2940 Ma [16].

The transition temperature from talc to anthophyllite in ultramafic rocks in the Bergell tonalite area (Italy) was determined to be around 650 °C by Trommsdorff and Connolly [41]. This estimate is compatible with the occurrence of talc for the given Seqi bulk-rock composition, which outlines a P–T range of less than 700 °C at below 1 GPa [5]. This field also allows for orthoamphibole to be stable within the same bulk rock as talc, which is indeed consistent with the observed petrography (Figure 6a).

From the above evidence, we can deduce that the talc formation in the Seqi olivine mine must have occurred at temperatures of 600–650 °C below 1 GPa at 2940 ± 5 Ma, and was associated with the intrusion of the late stage pegmatitic trondhjemite sheets.

5.2. Oxygen Isotope Constraints on the Origin and Temperature of Metasomatic Fluids

To further study the temperature of talc formation, we calculated $\delta^{18}O$ values of aqueous fluids that could have been in equilibrium with the talc, anthophyllite, and phlogopite samples at a range of temperatures, using available talc-water, anthophyllite-water, and phlogopite-water fractionation factors [42,43]. We also calculated $\delta^{18}O$ of aqueous fluids that could have been in equilibrium with the trondhjemite sample at different temperatures, based on the modal abundances of 80.61% albite, 18.99% quartz, and 0.4% biotite in the trondhjemite sample as determined by XRD analysis, using the available biotite-water, albite-water, and quartz-water fractionation factors by [44], [45] and [43], respectively. Depending on the talc-water fractionation factors that are used in the calculation, the calculated compositions of fluids that were potentially in equilibrium with the talc sample either range in $\delta^{18}O$ from 7 to 8‰ (c.f. the semi-empirical fractionation factors by Richter and Hoernes [42]) or, alternatively, they range from 5 to 6.5‰ (c.f., the theoretical fractionation factors by Zheng [43]). Whereas fluids with a $\delta^{18}O$ of 7 to 8‰ could have been derived from an intrusion that had a similar $\delta^{18}O$ as the trondhjemite sample, fluids with a $\delta^{18}O < 6.5$ could not have been derived from the trondhjemite sample at any temperature (Figure 11). We therefore suggest that the semi-empirical talc-water fractionation factors by Richter and Hoernes [42] more accurately correspond to the fractionation factors for the talc-water system that is studied here than the theoretical fractionation factors by Zheng [43]. The amount of early serpentinization experienced by the Seqi rocks is difficult to assess based on these oxygen isotope data, because the water/rock ratios at which serpentinization occurred are unknown. The $\delta^{18}O$ values of the dunite samples are similar to the values of typical mantle olivine, which would suggest that either low degrees of serpentinization could have occurred at high water/rock ratios or, alternatively, that high degrees of serpentinization could have occurred at low water/rock ratios.

The compositions of fluids that could have been in O isotope equilibrium with the talc, anthophyllite and phlogopite samples intersect at a $\delta^{18}O$ of ~8‰ within a temperature range of 600–700 °C (c.f. the talc-water fractionation factors by Richter and Hoernes [42] (Figure 11). The compositions of fluids that could have been derived from the trondhjemite sample also intersect this temperature range at a $\delta^{18}O$ of ~8‰. We therefore suggest that the talc, anthophyllite, and phlogopite samples could have formed at a temperature range of 600–700 °C from fluids that had a $\delta^{18}O$ of ~8‰, i.e., from fluids that could have been derived from the trondhjemite intrusion. The range of formation temperatures for the talc, anthophyllite, and phlogopite samples as reconstructed from their $\delta^{18}O$ values (600–700 °C)

is in good agreement with the temperature constraints from phase relations of the dunite bulk-rock composition (600–650 °C; see above).

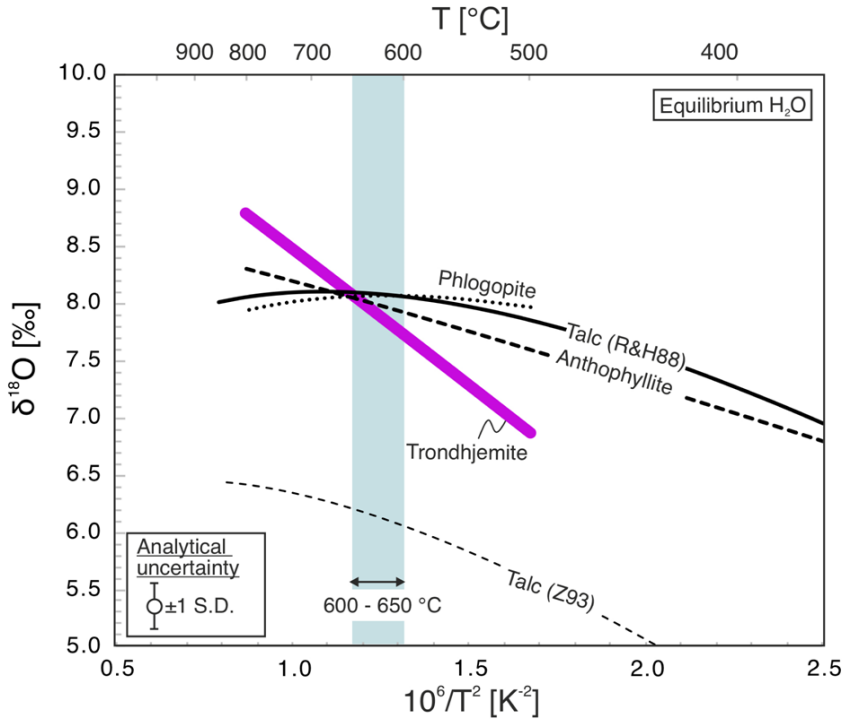

Figure 11. Calculated $\delta^{18}O$ of fluids that could have been in equilibrium with the mineral samples (indicated) and with the trondhjemite sample from this study. The fluid compositions were calculated from the measured $\delta^{18}O$ values of the samples (inset shows measurement precisions), in conjunction with available mineral-water fractionation factors [42–45]. The $\delta^{18}O$ of the trondhjemite sample was based on modal abundances of 80.61% albite, 18.99% quartz, and 0.4% biotite in the sample, as determined by XRD analysis. The suggested temperature range for talc formation from the phase relations of the dunite bulk-rock composition is shown by the vertical bar (600–650 °C; see text). R&H88 = Richter and Hoernes [42]; Z93 = Zheng [43].

The $\Delta'^{17}O_{0.528}$ values of the talc, anthophyllite, and phlogopite samples are similar to those of most igneous rocks and minerals (e.g., [21]), including the trondhjemite sample. This observation confirms that fluids that were involved in the formation of these particular samples were derived from magmatic waters with a $\Delta'^{17}O_{0.528}$ of about −40 ppm. In contrast, rocks that have become hydrothermally altered by fluids that were derived from seawater or from meteorite waters, for example, typically have $\delta^{18}O$ and $\Delta'^{17}O_{0.528}$ values that are lower and higher than igneous rocks, respectively (e.g., [21,46]).

5.3. Metasomatic Element Mobility

The mica zone stands out from the rest of the samples by having extreme enrichment in K_2O, and CaO even when compared to the granitoid pegmatite. This likely reflects local stabilization and scavenging from a fluid phase. However, the relatively immobile TiO_2, Al_2O_3, and heavy rare earth elements are also strongly enriched in the mica zone (Figure 9), which points to residual enrichment by dissolution of the pegmatite.

The anthophyllite and the talc zones, on the other hand, appear to have been derived directly from the dunite host, mainly by the addition of SiO_2 and loss of MgO and FeO^T. The relative loss of Ni in these metasomatic zones in comparison to the dunite precursor, likely reflects the breakdown of olivine and thus liberation of the compatible Ni hosted by this mineral. In contrast, Cr is enriched,

which appears to be related to the formation of chromite-magnetite solid solution by an immobilization of part of FeO^T from the dissolved olivine.

To quantify these compositional changes, we carried out isocon mass balance modelling [47,48] of the relevant sample pairs. It should be noted, however, that such modelling inherently has large uncertainties and only work under the assumption that the starting composition were identical for the samples that are being compared. Using TiO_2, Al_2O_3, and Y for the immobile reference line we find that the talc zone represents a net mass gain of about 37%, which was dominated by the addition of SiO_2, K_2O, Rb, Cs, as well as U, Th, and Cr, whereas MgO, FeO^T, and CaO were lost together with Ni and Sc.

In contrast, the amphibole zone represents a net mass loss of about −50% in comparison with the dunite precursor. The losses in this zone were dominated by the depletion in MgO, CaO, SiO_2 and FeO^T (in that order), despite relative gains in MnO, K_2O, Rb, Cs, and U.

Using only TiO_2 and Al_2O_3 to constrain the isocon regression line for the pegmatite and mica zone alteration pair, we found no meaningful solution. This is consistent with the extreme enrichment observed for immobile elements like TiO_2, Zr and the heavy rare earth elements.

The calculated mass changes from the dunite to the talc and amphibole zones are consistent with the chemical gradient of silica between a felsic pegmatite and the dunite host, which would promote the diffusion of SiO_2 from the amphibole zone into the talc zone. Both metasomatic zones experienced enrichment in K_2O and associated large ion lithophile elements. Interestingly, U was also enriched in both zones, which point to relatively oxidizing fluids that were able to move uranyl-complexes from the granitoid into the ultramafic host rock.

Regarding that both dunite and trondhjemite at Seqi are "dry" rocks, the metasomatic zone situated on their contact is most probably the fluid residual of the trondhjemite sheet crystallization. Its mineralogical characteristic is a transition from a phlogopite-dominated zone on the trondhjemite side to a talc-dominated one on the dunite side, with a specific thin middle zone formed of almost pure anthophyllite with oriented growth of crystals suggesting that it formed during the last stage of the process, filling the remaining narrow fracture. We noted that the observed characteristic mineralogy can be understood from the action of a silica rich fluid expelled from a crystallizing felsic melt on the dunite. Its reaction with dunite resulted in dissolution of olivine and crystallization of talc, with a net enrichment of residual fluid in Mg and Fe. This enrichment enabled nucleation of phlogopite on the trondhjemite side and, subsequently, with a decrease in water content, a crystallization of contemporary and ultimately the sole anthophyllite in the middle of the metasomatic zone. The gradients of some characteristic major elements in the metasomatic zone can be understood from this mineral result. Iron is incorporated in talc only in relatively small amounts, whereas both phlogopite and anthophyllite form solid solutions with corresponding Fe-rich end-members and readily took Fe released from dunite dissolution. Like Fe, anthophyllite readily incorporates Mn, as reflected in its gradient. Among the three main minerals of the metasomatic zone, phlogopite is the only host for Al and K, which explains their concentration in the mica zone. An interesting detail is a concentration of Ca in the metasomatic zone, resulting in crystallization of tremolite, rather than anthophyllite, close to the trondhjemite side. At the same time, Na is mostly absent from the metasomatic zone, obviously fully absorbed in the highly albitic plagioclase in trondhjemite.

6. Conclusions

The investigated metasomatic zone at the Archean Seqi Ultramafic Complex, SW Greenland, consists of three distinct mineral zones dominated by (1) talc, (2) anthophyllite, and (3) phlogopite, which were developed at the contact of an intrusive trondhjemite sheet in dunite. The following conclusions can be made based in the presented data:

(1) A zircon crystal inclusion in a large (4 cm) olivine porphyroblast was dated by in situ U–Pb isotope analysis, yielding a weighted mean $^{207}Pb/^{206}Pb$ age of 2963 ± 1 Ma, demonstrating dehydration and recrystallization of the ultramafic rocks at that time. In contrast, the 2940 ± 5 Ma zircon age of the

intrusive pegmatite was likely coincident with the development of the studied metasomatic talc zone at the Seqi Olivine Mine.

(2) Considering phase relations appropriate for the dunite bulk-rock composition, we deduced the talc forming conditions to be at temperatures of 600–650 °C and at a pressure below 1 GPa.

(3) Triple oxygen isotope data for talc, anthophyllite, and phlogopite in the metasomatic zones indicate formation in relation to fluids with a $\delta^{18}O$ of ~8‰ and a $\Delta'^{17}O_{0.528}$ of about −40 ppm at a temperature range of 600–700 °C. This conclusion supports a formation scenario involving fluids that were derived from the late stage pegmatitic trondhjemite intrusion.

(4) Absolute element mobility in the metasomatic zone points to a net mass gain of about 37% for the talc zone, involving the addition of SiO_2, K_2O, Rb, Cs, as well as U, Th, and Cr, whereas MgO, FeO^T, and CaO were lost together with Ni and Sc. In contrast, the amphibole zone had a net mass loss of about −50% in comparison with the dunite precursor. These losses were dominated by the depletion in MgO, CaO, SiO_2, and FeO^T, and relative gains in MnO, K_2O, Rb, Cs, and U. Thus, the overall mass transfer demonstrates uptake and transport of SiO_2, large ion lithophile elements (LILE) and K_2O into the dunite body, whereas MgO and FeO^T were lost during this metasomatic process. The mobility of U indicates relative oxidizing fluid conditions during talc formation in contrast to the strongly reduced fluids that characterize serpentinization processes.

Supplementary Materials: The following are available online at http://www.mdpi.com/2075-163X/10/1/85/s1, Figure S1: Talc zone PXRD diagram, Figure S2: Amphibole zone PXRD diagram, Figure S3: Mica zone PXRD diagram, Figure S4: Trondhjemite PXRD diagram, Figure S5: TIMA scan of olivine porphyroblast in sample 186460, Figure S6: Average U–Pb age plot for zircon in sample 186460, Table S1: Bulk-rock geochemical data, Table S2: Raw EMPA data, Table S3: Zircon U–Pb isotope data.

Author Contributions: Conceptualization, K.S. and T.B.-Z.; methodology, L.W., S.P., A.P., and C.L.K; writing—original draft preparation, L.W., K.S.; writing—review and editing, K.S.; funding acquisition, K.S. All authors have read and agreed to the published version of the manuscript.

Funding: This research including the APC was funded by VILLUM FONDEN, grant number 18978.

Acknowledgments: We thank three anonymous reviewers for their constructive comments, which improved the manuscript.

Conflicts of Interest: The authors declare no conflicts of interest.

References

1. Nutman, A.P.; McGregor, V.R.; Friend, C.R.; Bennett, V.C.; Kinny, P.D. The Itsaq gneiss complex of southern West Greenland; the world's most extensive record of early crustal evolution (3900–3600 Ma). *Precambrian Res.* **1996**, *78*, 1–39. [CrossRef]
2. Nutman, A.P.; Friend, C.R.; Hiess, J. Setting of the ~2560 Ma Qôrqut Granite complex in the Archean crustal evolution of southern west Greenland. *Am. J. Sci.* **2010**, *310*, 1081–1114. [CrossRef]
3. Szilas, K. A geochemical overview of mid-Archaean metavolcanic rocks from southwest Greenland. *Geosciences* **2018**, *8*, 266. [CrossRef]
4. Windley, B.F.; Garde, A.A. Arc-generated blocks with crustal sections in the North Atlantic craton of West Greenland: Crustal growth in the Archean with modern analogues. *Earth-Sci. Rev.* **2009**, *93*, 1–30. [CrossRef]
5. Szilas, K.; van Hinsberg, V.; McDonald, I.; Næraa, T.; Rollinson, H.; Adetunji, J.; Bird, D. Highly refractory Archaean peridotite cumulates: Petrology and geochemistry of the Seqi Ultramafic Complex, SW Greenland. *Geosci. Front.* **2018**, *9*, 689–9714. [CrossRef]
6. McIntyre, T.; Pearson, D.G.; Szilas, K.; Morishita, T. Implications for the origins of Eoarchean ultramafic rocks of the North Atlantic Craton: A study of the Tussaap Ultramafic complex, Itsaq Gneiss complex, southern West Greenland. *Contrib. Mineral. Petrol.* **2019**, *174*, 96. [CrossRef]
7. Keulen, N.; Schumacher, J.C.; Næraa, T.; Kokfelt, T.F.; Scherstén, A.; Szilas, K.; van Hinsberg, V.J.; Schlatter, D.M.; Windley, B.F. Meso-and Neoarchaean geological history of the Bjørnesund and Ravns Storø Supracrustal Belts, southern West Greenland: Settings for gold enrichment and corundum formation. *Precambrian Res.* **2014**, *254*, 36–58. [CrossRef]

8. Yakymchuk, C.; Szilas, K. Corundum formation by metasomatic reactions in Archean metapelite, SW Greenland: Exploration vectors for ruby deposits within high-grade greenstone belts. *Geosci. Front.* **2018**, *9*, 727–9749. [CrossRef]
9. Szilas, K.; Kelemen, P.B.; Bernstein, S. Peridotite enclaves hosted by Mesoarchaean TTG-suite orthogneisses in the Fiskefjord region of southern West Greenland. *GeoResJ* **2015**, *7*, 22–34. [CrossRef]
10. Friend, C.R.; Nutman, A.P. New pieces to the Archaean terrane jigsaw puzzle in the Nuuk region, southern West Greenland: Steps in transforming a simple insight into a complex regional tectonothermal model. *J. Geol. Soc.* **2005**, *162*, 147–162. [CrossRef]
11. Garde, A.A. Accretion and evolution of an Archaean high-grade grey gneiss—Amphibolite complex: The Fiskefjord area, southern West Greenland. *Geol. Greenl. Surv. Bull.* **1997**, *177*, 115.
12. Garde, A.A.; Friend, C.R.; Nutman, A.P.; Marker, M. Rapid maturation and stabilisation of middle Archaean continental crust: The Akia terrane, southern West Greenland. *Bull. Geol. Soc. Den.* **2000**, *47*, 1–27.
13. Gardiner, N.J.; Kirkland, C.L.; Hollis, J.; Szilas, K.; Steenfelt, A.; Yakymchuk, C.; Heide-Jørgensen, H. Building Mesoarchaean crust upon Eoarchaean roots: The Akia Terrane, West Greenland. *Contrib. Mineral. Petrol.* **2019**, *174*, 20. [CrossRef]
14. Garde, A.A. A mid-Archaean island arc complex in the eastern Akia terrane, Godthåbsfjord, southern West Greenland. *J. Geol. Soc.* **2007**, *164*, 565–579. [CrossRef]
15. Szilas, K.; Tusch, J.; Hoffmann, J.E.; Garde, A.A.; Münker, C. Hafnium isotope constraints on the origin of Mesoarchaean andesites in southern West Greenland, North Atlantic craton. *Geol. Soc. Lond. Spec. Publ.* **2017**, *449*, 19–38. [CrossRef]
16. Yakymchuk, C.; Kirkland, C.; Hollis, J.; Kendrick, J.; Gardiner, N.; Szilas, K. Mesoarchean partial melting of mafic crust and tonalite production during high-T–low-P stagnant tectonism, Akia Terrane, West Greenland. *Precambrian Res.* **2019**, in press. [CrossRef]
17. Washington State University GeoAnalytical Lab. Technical Notes Describing Sample Preparation, Analytical Procedure, Precision, and Accuracy of XRF and ICP-MS Analysis. Website Visited on 29 November 2019. Available online: https://environment.wsu.edu/facilities/geoanalytical-lab/technical-notes/ (accessed on 20 January 2020).
18. Waight, T.E.; Tørnqvist, J.B. Sr isotope zoning in plagioclase from andesites at Cabo De Gata, Spain: Evidence for shallow and deep contamination. *Lithos* **2018**, *308*, 159–167. [CrossRef]
19. Pack, A.; Tanaka, R.; Hering, M.; Sengupta, S.; Peters, S.; Nakamura, E. The oxygen isotope composition of San Carlos olivine on the VSMOW2-SLAP2 scale. *Rapid Commun. Mass Spectrom.* **2016**, *30*, 1495–1504. [CrossRef]
20. Pack, A.; Herwartz, D. The triple oxygen isotope composition of the Earth mantle and understanding $\Delta^{17}O$ variations in terrestrial rocks and minerals. *Earth Planet. Sci. Lett.* **2014**, *390*, 138–145. [CrossRef]
21. Sharp, Z.D.; Wostbrock, J.A.G.; Pack, A. Mass-dependent triple oxygen isotope variations in terrestrial materials. *Geochem. Perspect. Lett.* **2018**, *7*, 27–31. [CrossRef]
22. Valley, J.W.; Kitchen, N.; Kohn, M.J.; Niendorf, C.R.; Spicuzza, M.J. UWG-2, a garnet standard for oxygen isotope ratios: Strategies for high precision and accuracy with laser heating. *Geochim. Cosmochim. Acta* **1995**, *59*, 5223–5231. [CrossRef]
23. Stern, R.A.; Bodorkos, S.; Kamo, S.L.; Hickman, A.H.; Corfu, F. Measurement of SIMS instrumental mass fractionation of Pb isotopes during zircon dating. *Geostand. Geoanal. Res.* **2009**, *33*, 145–168. [CrossRef]
24. Wiedenbeck, M.A.; Alle, P.; Corfu, F.; Griffin, W.L.; Meier, M.; Oberli, F.V.; Quadt, A.V.; Roddick, J.C.; Spiegel, W. Three natural zircon standards for U–Th–Pb, Lu–Hf, trace element and REE analyses. *Geostand. Newsl.* **1995**, *19*, 1–23. [CrossRef]
25. Jackson, S.E.; Pearson, N.J.; Griffin, W.L.; Belousova, E.A. The application of laser ablation-inductively coupled plasma-mass spectrometry to in situ U–Pb zircon geochronology. *Chem. Geol.* **2004**, *211*, 47–69. [CrossRef]
26. Sláma, J.; Košler, J.; Condon, D.J.; Crowley, J.L.; Gerdes, A.; Hanchar, J.M.; Horstwood, M.S.; Morris, G.A.; Nasdala, L.; Norberg, N.; et al. Plešovice zircon—A new natural reference material for U–Pb and Hf isotopic microanalysis. *Chem. Geol.* **2008**, *249*, 1–35. [CrossRef]
27. Paton, C.; Hellstrom, J.; Paul, B.; Woodhead, J.; Hergt, J. Iolite: Freeware for the visualisation and processing of mass spectrometric data. *J. Anal. At. Spectrom.* **2011**, *26*, 2508–2518. [CrossRef]

28. Sun, S.S.; McDonough, W.F. Chemical and isotopic systematics of oceanic basalts: Implications for mantle composition and processes. *Geol. Soc. Lond. Spec. Publ.* **1989**, *42*, 313–345. [CrossRef]
29. Bindeman, I. Oxygen isotopes in mantle and crustal magmas as revealed by single crystal analysis. *Rev. Mineral. Geochem.* **2008**, *69*, 445–478. [CrossRef]
30. Mattey, D.; Lowry, D.; Macpherson, C. Oxygen isotope composition of mantle peridotite. *Earth Planet. Sci. Lett.* **1994**, *128*, 231–241. [CrossRef]
31. Guotana, J.; Morishita, T.; Yamaguchi, R.; Nishio, I.; Tamura, A.; Tani, K.; Harigane, Y.; Szilas, K.; Pearson, D. Contrasting textural and chemical signatures of chromitites in the Mesoarchaean Ulamertoq peridotite body, southern West Greenland. *Geosciences* **2018**, *8*, 328. [CrossRef]
32. Nishio, I.; Morishita, T.; Szilas, K.; Pearson, G.; Tani, K.I.; Tamura, A.; Harigane, Y.; Guotana, J.M. Titanian Clinohumite-Bearing Peridotite from the Ulamertoq Ultramafic Body in the 3.0 Ga Akia Terrane of Southern West Greenland. *Geosciences* **2019**, *9*, 153. [CrossRef]
33. Kirkland, C.L.; Yakymchuk, C.; Szilas, K.; Evans, N.; Hollis, J.; McDonald, B.; Gardiner, N.J. Apatite: A U-Pb thermochronometer or geochronometer? *Lithos* **2018**, *318*, 143–157. [CrossRef]
34. Cochrane, R.; Spikings, R.A.; Chew, D.; Wotzlaw, J.F.; Chiaradia, M.; Tyrrell, S.; Schaltegger, U.; Van der Lelij, R. High temperature (>350 °C) thermochronology and mechanisms of Pb loss in apatite. *Geochim. Cosmochim. Acta* **2014**, *127*, 39–56. [CrossRef]
35. Schoene, B.; Bowring, S.A. Determining accurate temperature–time paths from U–Pb thermochronology: An example from the Kaapvaal craton, southern Africa. *Geochim. Cosmochim. Acta* **2007**, *71*, 165–185. [CrossRef]
36. Nutman, A.P.; Rivers, T.; Longstaffe, F.; Park, J.F. The Ataneq fault and mid-Proterozoic retrograde metamorphism of early Archaean tonalites of the Isukasia area, southern West Greenland: Reactions, fluid compositions and implications for regional studies. In *Fluid Movements—Element Transport and the Composition of the Deep Crust*; Springer: Dordrecht, The Netherlands, 1989; pp. 151–170.
37. Friend, C.R.; Nutman, A.P.; Baadsgaard, H.; Kinny, P.D.; McGregor, V.R. Timing of late Archaean terrane assembly, crustal thickening and granite emplacement in the Nuuk region, southern West Greenland. *Earth Planet. Sci. Lett.* **1996**, *142*, 353–365. [CrossRef]
38. Nutman, A.P.; Christiansen, O.; Friend, C.R. 2635 Ma amphibolite facies gold mineralisation near a terrane boundary (suture?) on Storø, Nuuk region, southern West Greenland. *Precambrian Res.* **2007**, *159*, 19–32. [CrossRef]
39. Scherstén, A.; Szilas, K.; Creaser, R.A.; Næraa, T.; van Gool, J.A.; Østergaard, C. Re–Os and U–Pb constraints on gold mineralisation events in the Meso- to Neoarchaean Storø greenstone belt, Storø, southern West Greenland. *Precambrian Res.* **2012**, *200*, 149–162. [CrossRef]
40. Szilas, K.; van Hinsberg, V.J.; McDonald, I.; Morishita, T.; Pearson, D.G. Highly depleted peridotites within Mesoarchaean orthogneiss at the Seqi Olivine Mine, SW Greenland—Potential implications for the formation of cratonic keels. *Goldschmidt Conf. Abstr. Yokohama* **2016**, *3009*, 1.
41. Trommsdorff, V.; Connolly, J.A. The ultramafic contact aureole about the Bregaglia (Bergell) tonalite: Isograds and a thermal model. *Schweiz. Mineral. Und Petrogr. Mitt.* **1996**, *76*, 537–547.
42. Richter, R.; Hoernes, S. The application of the increment method in comparison with experimentally derived and calculated O-isotope fractionations. *Chem. Erde* **1988**, *48*, 1–18.
43. Zheng, Y.F. Calculation of oxygen isotope fractionation in hydroxyl-bearing silicates. *Earth Planet. Sci. Lett.* **1993**, *120*, 247–263. [CrossRef]
44. Matsuhisa, Y.; Goldsmith, J.R.; Clayton, R.N. Oxygen isotopic fractionation in the system quartz-albite-anorthite-water. *Geochim. Cosmochim. Acta* **1979**, *43*, 1131–1140. [CrossRef]
45. Bottinga, Y.; Javoy, M. Comments on oxygen isotope geothermometry. *Earth Planet. Sci. Lett.* **1973**, *20*, 250–265. [CrossRef]
46. Peters, S.T.M.; Szilas, K.; Pack, A.; Sengupta, S.; Kirkland, C.; Gabe-Schönberg, D. Oxygen isotope compositions of >2.7 Ga aqueous fluids recorded in metamorphic peridotites from southeast Greenland. *Earth Planet. Sci. Lett.* **2020**. in review.

47. Grant, J.A. The isocon diagram; a simple solution to Gresens' equation for metasomatic alteration. *Econ. Geol.* **1986**, *81*, 1976–1982. [CrossRef]
48. López-Moro, F.J. EASYGRESGRANT—A Microsoft Excel spreadsheet to quantify volume changes and to perform mass-balance modeling in metasomatic systems. *Comput. Geosci.* **2012**, *39*, 191–196. [CrossRef]